Available online at www.sciencedirect.com
ScienceDirect
Journal of Solid State Chemistry 180 (2007) 2566–2576
JOURNAL OF SOLID STATE CHEMISTRY
www.elsevier.com/locate/jssc

Crystal chemistry and thermodynamic properties of anisotropic $Ce_2Ni_7H_{4.7}$ hydride

R.V. Denys[a,b], V.A. Yartys[a,*], Masashi Sato[c], A.B. Riabov[a,b], R.G. Delaplane[a,d,1]

[a]*Institute for Energy Technology, P.O. Box 40, Kjeller NO-2027, Norway*
[b]*Physico-Mechanical Institute of the National Academy of Science of Ukraine, 5 Naukova Street, Lviv 79601, Ukraine*
[c]*Department of Applied Chemistry, School of Engineering, Tokai University, 1117 Kita-Kaname, Hiratsuka, Kanagawa 259-1292, Japan*
[d]*The Studsvik Neutron Research Laboratory, Uppsala University, S-611 82 Nyköping, Sweden*

Received 26 April 2007; received in revised form 25 June 2007; accepted 2 July 2007
Available online 10 August 2007

Abstract

A new intermetallic deuteride $Ce_2Ni_7D_{4.7}$ with an anomalous volume expansion has been studied. Its structure was solved on the basis of *in situ* neutron diffraction data. Expansion proceeds along the *c*-axis and within the $CeNi_2$ slabs only. All D atoms are located inside these slabs and on the border between $CeNi_2$ and $CeNi_5$. Ordering of D atoms in the bulk of $CeNi_2$ is accompanied by substantial deformation of these slabs thus lowering the hexagonal symmetry to orthorhombic [space group *Pmcn* (No. 62); $a = 4.9251(3)$ Å, $b = 8.4933(4)$ Å, $c = 29.773(1)$ Å]. Inside the $CeNi_2$ layer the hydrogen sublattice is completely ordered; all D–D distances exceed 2.0 Å. Local coordination of Ni by D inside the $CeNi_2$ blocks is of "open", saddle-like type. Hydrogen ordering is mainly determined by Ce–H and H–H interactions. The pressure–composition–temperature measurements yielded the following thermodynamic parameters of the formation of the hydride: $\Delta H = -22.4\,kJ/mol_H$, $\Delta S = -59.9\,J/(K\,mol_H)$.

Keywords: Metal hydrides; Crystal structure and symmetry; Neutron diffraction; Pressure–composition–temperature relationships

1. Introduction

The hydrogenation of intermetallic alloys is utilised for the storage of atomic, interstitial H thus providing a high-volume density of stored hydrogen. The crystal chemistry of the corresponding hydrides can be related to their hydrogen storage characteristics that can be applied for the optimisation of H storage performance.

Typically, for intermetallic hydrides the metal lattice is modestly modified with the accommodation of hydrogen atoms into the available interstitial vacancies; the interatomic metal–metal distances change by only a few percent. However, recent studies have shown the existence of "anisotropic" RE–Ni-based hydrides (RE = rare-earth metal) where a large expansion occurs along a single crystallographic direction [1], and very small changes in directions normal to this expansion take place. Earlier, there were reported data on the crystal structures of $CeNi_3D_{2.8}$ [2], $LaNi_3D_{2.8}$ [3], $CeY_2Ni_9D_{7.7}$ [4] and $La_2Ni_7D_{6.5}$ [1] that are related to the $RENi_3$ and RE_2Ni_7 intermetallics [5]. The structures of the initial intermetallic alloys are built up from two types of metal slabs, $RENi_5$ ($CaCu_5$ type) and $RENi_2$ ($MgZn_2$ type) that are stacked along $[001]_{hex}$. The combination $1 \times RENi_5 + 2 \times RENi_2$ gives the overall stoichiometry $3 \times RENi_3$, and for the RE_2Ni_7 compounds the ratio of the $RENi_5$ to $RENi_2$ slabs is 1:1.

During the hydrogenation process to form $CeNi_3D_{2.8}$ [2], $LaNi_3D_{2.8}$ [3] and $La_2Ni_7D_{6.5}$ [1], common and unusual structural features are observed:

- The lattice expansion proceeds within the $RENi_2$ slabs only and is confined to [001]. Such expansion amounts to 58–63% and is associated with occupation by D atoms of the Laves-phase layers.
- The $RENi_5$ slabs remain unoccupied by D. This correlates with absence of the lattice expansion of these layers.

*Corresponding author. Fax: +47 63 81 29 05.
E-mail address: volodymyr.yartys@ife.no (V.A. Yartys).
[1]Present address: Borgdalsgången 36, SE-611 57 Nyköping, Sweden.

0022-4596/$ - see front matter © 2007 Elsevier Inc. All rights reserved.
doi:10.1016/j.jssc.2007.07.002

- New types of interstitial sites occupied by D are formed because of anisotropic expansion, namely RE_3Ni_3 octahedra and RE_3Ni tetrahedra. In addition to these sites, D enters RE_2Ni_2 tetrahedra belonging to both $RENi_5$ and $RENi_2$ layers.
- An ordered hydrogen sublattice is formed in $CeNi_3D_{2.8}$ and $La_2Ni_7D_{6.5}$. The structural behaviour of $CeNi_3D_{2.8}$ and $La_2Ni_7D_{6.5}$ is dominated by RE–H and H–H interactions.

The present work is focused on studies of the thermodynamics and crystal structure of $Ce_2Ni_7H(D)_{4.7}$, which is chemically related to $La_2Ni_7D_{6.5}$. The goal of this study is to gain a better understanding of the structural and physical–chemical properties of anisotropic hydrides. While writing this manuscript, we became aware that a similar orthorhombic Ce_2Ni_7-based hydride and deuteride have been independently studied by Filinchuk et al. [6]. They have confirmed the typical group behaviour for anisotropic hydrides [1–4] of the transformation of the metallic sublattice during hydrogenation (elongation along [001], with only the Laves-phase blocks becoming enlarged). As the main conclusion, a tetrahedral NiD_4 coordination of Ni atoms within the $CeNi_2$ blocks has been reported [6]. We will show later in this paper that formation of NiD_4 tetrahedra contradicts the findings of the present study, where a different, saddle-type ordering of four H atoms around Ni was found. A significantly different deuterium substructure and smaller deuterium content (4.1 at. D/Ce_2Ni_7) were reported [6] compared to the findings of the present study where deuterides with 4.4 and 4.7 at. D/f.u. have been investigated. Possible reasons for the disagreements between Ref. [6] and the present work could be in the experimental conditions employed in [6] (exposure of the studied hydrides to air leading to their partial oxidation) as compared to the present work (*in situ* diffraction experiment under the pressure of deuterium gas allowing to study the material at equilibrium conditions). These variations in the experimental conditions will be proposed to account for the differences between the results of the two studies.

2. Experimental

2.1. Sample synthesis and characterisation

The Ce_2Ni_7 alloy was prepared by arc melting of bulk metals Ce (99.9%) and Ni (99.95%) under argon atmosphere followed by annealing in evacuated quartz ampoules at 1073 K for 2 weeks and then quenching in cold water. XRD characterisation with a DRON 3.0 X-ray diffractometer (Cu$K\alpha$ radiation) showed the alloy to be single-phase containing no detectable impurities. From the X-ray diffraction profile, a hexagonal unit cell was derived with $a = 4.9419(9)$ Å, $c = 24.508(5)$ Å, $V = 518.36(17)$ Å^3 which agrees well with published values [5,7].

All handling of the sample was done in a glove box in an inert argon atmosphere. For the preparation of the deuteride the sample was crushed in an agate mortar, loaded in a stainless steel autoclave (tube wall thickness 0.1 mm, $d_{inner} = 4$ mm), and activated by heating in vacuum up to 673 K followed by cooling to room temperature. Then the autoclave was slowly filled with 0.1 MPa D_2 (99.8% purity). The deuteration process was rather fast, and after saturation, reached within 1 min, the pressure was increased up to 2 MPa. The final product was a single-phase deuteride of 4.70 ± 0.05 at. D/Ce_2Ni_7 that was already reached at 0.1 MPa of pressure.

After PND measurements described below, deuterium was completely desorbed from the material; the sample was filled into a 0.3 mm glass capillary for SXRD analysis. Measurement was carried out at the high-resolution powder diffraction station BM01B at the Swiss–Norwegian Beam Lines at ESRF ($\lambda = 0.37504(1)$ Å, Debye–Scherrer geometry, 2Θ step size 0.0025°). Refined unit cell parameters of Ce_2Ni_7 agree well with those determined for the initial alloy: $a = 4.94131(3)$ Å; $c = 24.5136(2)$ Å; $V = 518.349(6)$ Å^3.

2.2. Neutron powder diffraction

After synthesis, powder neutron diffraction (PND) data were immediately collected with the high-resolution R2D2 diffractometer ($\lambda = 1.551(1)$ Å, 2Θ step size 0.05°) at the Studsvik Neutron Research Laboratory, Uppsala University, Sweden [8]. The instrument calibration parameters and wavelength of the neutron beam were determined by a least-squares fit for diffraction data collected for the standard reference materials; Si, NIST 640c and Al_2O_3, NIST 676 [8]. The preparation laboratory was located in annex to the Studsvik R2 reactor hall that ensured a minimum delay from sample preparation to the diffraction measurements. After the PND *in situ* measurement (in the stainless steel autoclave under 2 MPa D_2) the deuteride was reloaded from the autoclave into a vanadium sample holder with an inner diameter of 5 mm. The reloading was done in a glove box under a purified argon atmosphere, and the vanadium container was sealed with indium wire. A new *ex situ* PND data set was then collected with R2D2.

The GSAS program [9] was used for the Rietveld profile refinements of the crystal structure parameters of the initial intermetallic alloy and the prepared deuteride. Reflections from the stainless steel autoclave (space group $Fm\bar{3}m$; $a = 3.597$ Å) were excluded from the *in situ* PND profile during refinements. Neutron scattering lengths of the elements were taken from GSAS library: $b_{Ce} = 4.84$ fm; $b_{Ni} = 10.3$ fm; $b_D = 6.67$ fm.

2.3. Measurement of pressure–composition–temperature relationships for Ce_2Ni_7–H_2

Pressure–composition–temperature (PCT) relationships for the Ce_2Ni_7–H_2 system were measured by the Sieverts'

method on the sample used for the PND experiments after complete desorption of the deuterium to reform again the intermetallic Ce_2Ni_7 alloy. The sample was activated in vacuum at 573 K for 1 h, cooled under vacuum to 298 K and then slowly charged with hydrogen gas ($P_{H_2} = 1$ MPa). To achieve reproducible kinetics of hydrogen uptake and release, several absorption–desorption cycles were performed before measuring the isotherms. The purity grade of hydrogen gas used was 99.999%. The cycling has been done at the low temperature of 273 K in order to avoid a possible disproportionation of the Ce_2Ni_7 alloy. The measurements of the isotherms were performed in the temperature range 293–333 K and with hydrogen pressures from 10^{-3} to 10^{-1} MPa. An equilibrium state was considered to have been reached when the pressure change became less than 10^{-5} MPa.

3. Results and discussion

3.1. Thermodynamics studied by PCT isotherms

Fig. 1a shows the measured pressure–composition–temperature diagrams for the Ce_2Ni_7–H systems at temperatures between 293 and 333 K. The presence of a rather flat plateau is clearly seen at approximately $0.2 < H/Ce_2Ni_7 < 4.4$, which agrees well with an earlier report described in [10]. The isotherms saturate in the vicinity of 4.4–4.6 H/Ce_2Ni_7; the hydrogen solid solution limit is about $H/Ce_2Ni_7 = 0.2$. The limiting maximum hydrogen content in the hydride is close to 4.7 at. H/f.u. at 293 K, the experimental conditions for the PND experiment. Hysteresis between the absorption and desorption measured ($P_{abs}/P_{des} = 1.2$ at 313 K) is relatively modest.

Based on the obtained isotherms, the van't Hoff plots in the plateau regions are shown for the H_2 absorption and desorption processes in Fig. 1b. The equilibrium pressure on the plateau region for the present work is slightly lower than the pressure reported by van Essen and Buschow [10]. The Ce_2Ni_7 alloy is relatively unstable with respect to the disproportionation process; therefore, to avoid decomposition, rather modest hydrogenation pressures below 1 MPa were applied (these pressures were much higher in [10], 4 MPa).

Changes of enthalpy ΔH_H and entropy ΔS_H as a function of H content are shown in Fig. 2a and b, respectively. The shape of the curves is very typical for the metal–hydrogen systems [11]. The ΔH_H and ΔS_H values are nearly constant: -22.4 ± 0.5 kJ/mol$_H$ and -59.9 ± 0.4 J/(K mol$_H$), respectively, for the range $0.5 < H/Ce_2Ni_7 < 3.2$; both values increase at H content exceeding 3.2.

Calculated thermodynamic properties of the Ce_2Ni_7–H_2 system in the pressure plateau area are summarised in Table 1. The reference data for the hydrides of the Ce–Ni and Ce–Co binary intermetallics are also included for comparison. It is interesting to note that, despite of significant differences in the Ce/Ni ratios, the heat of formation, ΔH_H, is very close for the $CeNi_3$- and Ce_2Ni_7-based hydrides, −22.4 and −22.6 kJ/mol$_H$, respectively. This feature, perhaps, has roots in preferential accommodation of hydrogen by the $CeNi_2$ layers in both structures, and will be discussed later in this paper. Furthermore, we note a very unusual alteration of the thermodynamics of hydrogen–metal interaction for the related Co- and Ni-containing binary intermetallics, respectively, $CeNi_3$ and $CeCo_3$, Ce_2Ni_7 and Ce_2Co_7. Indeed, for the conventional interstitial-type intermetallic hydrides, Co-containing systems are characterised by a higher thermal stability of the hydrides and, correspondingly lower values of

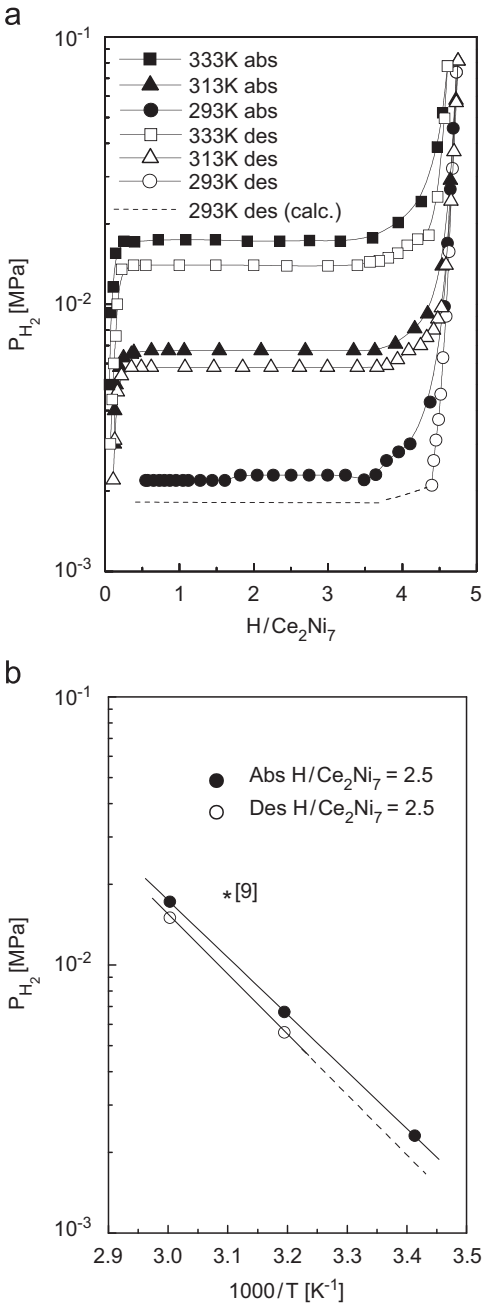

Fig. 1. (a) Absorption–desorption isotherms for the system Ce_2Ni_7–H_2. (b) van't Hoff plots lp P vs. $1/T$.

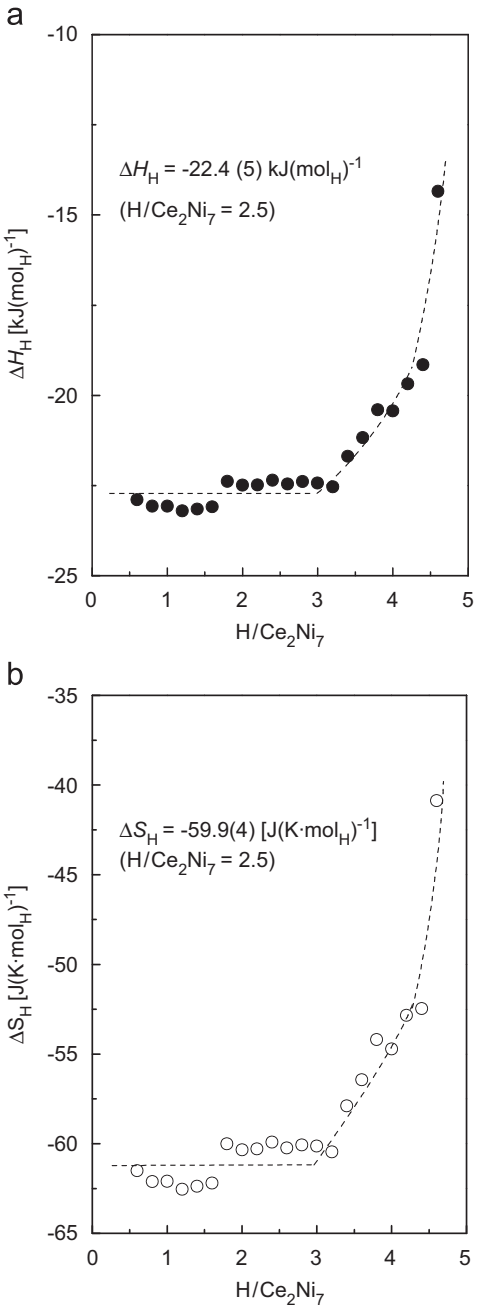

Fig. 2. Enthalpy (a) and entropy (b) changes with H content in the system Ce_2Ni_7–H_2.

enthalpies of the hydrogenation ΔH_H (see Table 1 where the data for such "conventional" $CeNi_5$- and $CeCo_5$-based hydrides are given). In contrast, an opposite trend is observed for the pairs of anisotropic hydrides, Ce_2Ni_7–Ce_2Co_7 and $CeNi_3$–$CeCo_3$. From the data given in Table 1, it is seen that (a) the ΔH_H values are similar for Ni and Co compounds with stoichiometries Ce/Ni(Co) = 1/3 or 2/7; (b) the Ni-based hydrides have slightly, yet significantly higher thermal stabilities. These observations clearly reflect the unusual behaviours of the anisotropic hydrides, which can be related to their crystal structure features.

Table 1
Thermodynamic properties of the Ce-based intermetallic hydrides

Hydride	Plateau pressure (MPa)	ΔH_H (kJ/mol$_H$)	Reference
$Ce_2Ni_7H_{4.7}$	0.017 (333 K)	-22.4 ± 0.5	Present work
$Ce_2Ni_7H_{4.4}$	0.02 (323 K)	-21.6[a]	[9]
$Ce_2Co_7H_{6.4}$	0.05 (323 K)	-20.3[a]	[9]
$CeNi_3H_3$	0.009 (323 K)	-22.6[a]	[9]
$CeCo_3H_{4.2}$	0.02 (323 K)	-21.5[a]	[9]
$CeNi_5H_6$	4.9 (298 K)	-7.1	[11]
$CeCo_5H_{2.6}$	0.13 (296 K)	-19.5	[11]
$CeNi_2H_4$	$<10^{-4}$ (298 K)	-27	[9,12]

[a]The partial molar enthalpy data were calculated based on the assumption that the partial molar entropy value is dominated by the dissociation from H_2 molecules to H atoms, -60 J/(K mol$_H$).

3.2. Crystal structure of the deuteride

In situ neutron diffraction data of the deuteride, indexed using a hexagonal unit cell (space group $P6_3/mmc$; $a = 4.9151(2)$ Å; $c = 29.776(2)$ Å), showed a pronounced (21.5%) expansion along [001] compared to the Ce_2Ni_7 intermetallic alloy ($\Delta V/V = 20.1\%$). Smaller unit cell parameters for the deuteride were obtained from *ex situ* PND data ($a = 4.9009(2)$ Å, $c = 29.633(2)$ Å), indicating a partial deuterium desorption from the sample.

Rietveld profile refinements of both *in situ* and *ex situ* PND data in the hexagonal setting revealed that unit cell expansion proceeds within the $CeNi_2$ slabs only (62–63%) with the $CeNi_5$ units remaining unchanged. Furthermore, such an uneven deformation of the metal sublattice is in agreement with deuterium occupancy of these structure fragments. Using difference Fourier analysis, we found D atoms distributed among six crystallographic sites with three chemically different metal atom surroundings, including Ce_3Ni_3, Ce_3Ni and Ce_2Ni_2. In general, the structures of $Ce_2Ni_7D_{4.4}$ and $Ce_2Ni_7D_{4.7}$ resemble that of the hexagonal $La_2Ni_7D_{6.5}$ [1]; as in other anisotropic hydrides, all D sites are located inside the $CeNi_2$ slabs or in the Ni nets connecting the $CeNi_2$ and $CeNi_5$ layers.

However, refinements in the hexagonal setting revealed the presence of significant features, which are impossible to explain unless the symmetry is assumed to be lowered from a hexagonal to an orthorhombic space group. These features included:

(a) The shift of a Ni1 atom located in the middle of $CeNi_2$ slab along hexagonal *c*-axis, described as splitting of the initial 2*a* site (0, 0, 0) into a 50% occupied 4*e* (0, 0, *z*) site with a distance of 1.4 Å between the sites.

An attempt to describe this feature as an anisotropic thermal displacement of Ni in the 2*a* site gave unreliably high U_{aniso} values along the hexagonal *c*-axis, $u_{33} = 0.80(8)$ Å^2 ($u_{11} = 0.011(6)$ Å^2, $u_{22} = 0.011(5)$ Å^2, $u_{12} = 0.005(3)$ Å^2).

(b) Unrealistically high isotropic displacement parameter for Ce1 atom located in the $CeNi_2$ slab ($U_{iso} = 0.066$ Å^2).

(c) 50% occupancy of the Ce_3Ni sites formed with a participation of a "split" Ni atom. These interstices do not exist in the parent intermetallic structure and are formed as a result of strong anisotropic expansion of the $CeNi_2$ slab. A 50% occupancy of this site together with a 50% occupancy of the split Ni1 site indicate possible ordering of D atoms.

From group–subgroup relations, $P6_3/mmc$–$Cmcm$, an orthorhombic unit cell with metrics $a_{orth} = a_{hex}$, $b_{orth} = a_{hex} + 2b_{hex}$, $c_{orth} = c_{hex}$ was first tested. However, it was rejected, as a description of the observed splitting of the Ni1 site was not possible. A completely ordered metal matrix substructure and successful description of the hydrogen sublattice were obtained when the symmetry of the structure was additionally lowered to the symmetry related to *Cmcm* orthorhombic space group *Pmcn*.

A model of the structure in the *Pmcn* space group contained 4 Ce sites, 11 Ni sites and 20 D sites. 11 from 20 D sites were rejected and the structure model with 9 occupied D sites and ordered D sublattice was found, giving an excellent fit to both *in situ* and *ex situ* PND data (see Fig. 3a and b).

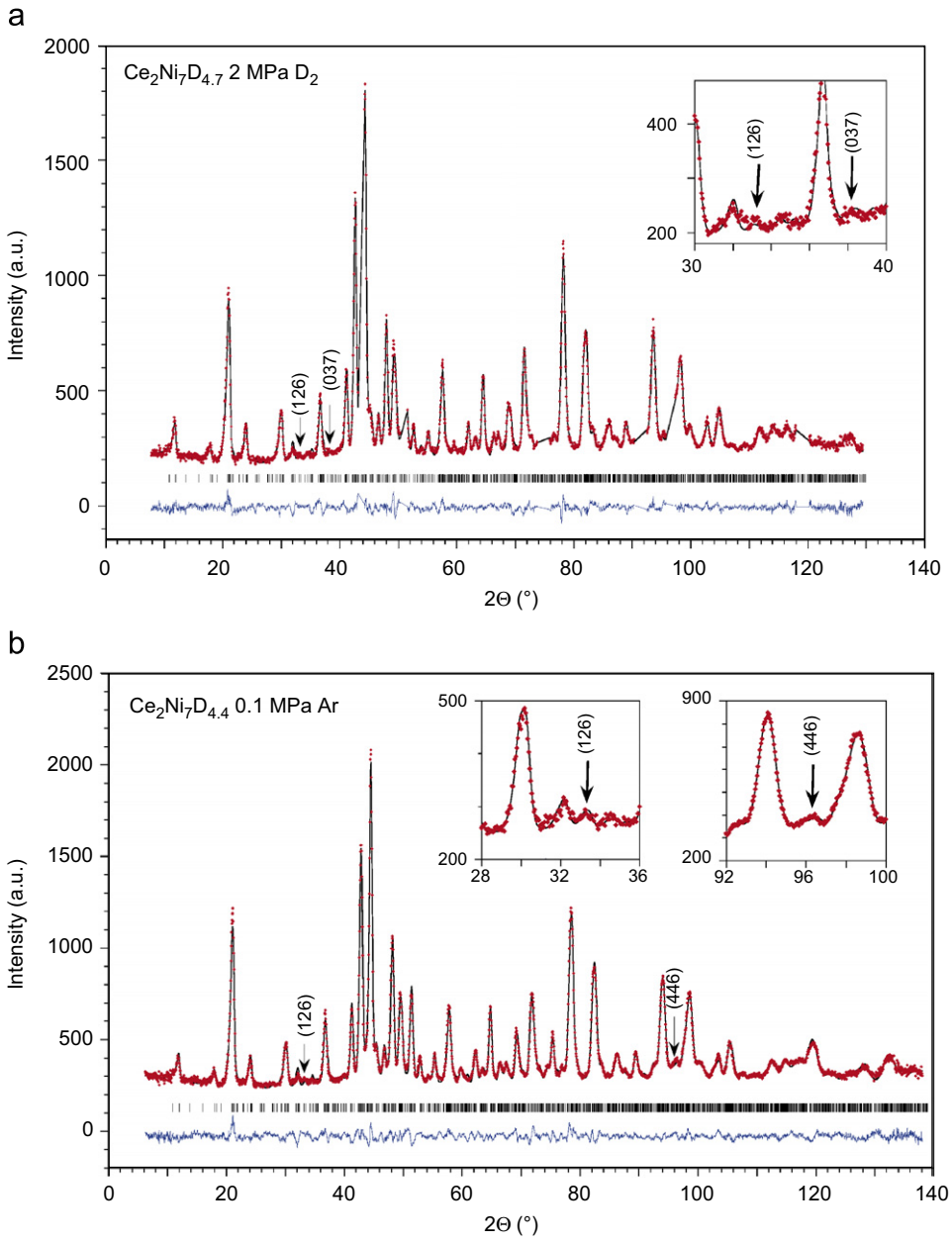

Fig. 3. Observed (dots), calculated (upper line) and difference (lower line) powder neutron diffraction profiles of the Ce_2Ni_7-based deuterides ($\lambda = 1.551(1)$ Å): (a) *in situ* measurement (2Θ angular ranges where contributions from the stainless steel autoclave were observed, 43.2–44.2; 50.35–51.55; 73.85–75.85; 90.35–92.5; 95.8–97.3 and 118.05–120.2, were excluded from the refinements); (b) *ex situ* measurement. Insets show the regions with superstructure peaks.

The final refinement showed a very small orthorhombic distortion of the deuteride structure for both data sets: $(b_{orth}/\sqrt{3}-a_{orth})/a_{orth} \approx -0.5\%$. Apparently, the peak splitting caused by such a small orthorhombic distortion cannot be clearly seen in the neutron diffraction pattern; however, a presence of weak reflections violating the hexagonal symmetry confirms the orthorhombic deformation of the structure. The most distinct of these peaks are marked in Fig. 3. The unit cell parameters for the orthorhombic structure are summarised in Table 2 and compared to those of parent Ce_2Ni_7 structure. Atomic parameters for the Ce_2Ni_7 structure (Table 3) were obtained from the Rietveld refinement of the SXRD pattern for the sample after complete deuterium desorption (confirmed by thermal desorption spectroscopy measurements of the studied sample).

A sample stoichiometry of $Ce_2Ni_7D_{4.65(9)}$ was obtained for *in situ* PND data and $Ce_2Ni_7D_{4.43(9)}$ for the *ex situ* experiments, respectively. Both values fit the stochiometric range obtained by PCT measurements where the limiting maximum hydrogen content is about 4.7 at. H/f.u. (see Section 3.1). Atomic positions in the structure of $Ce_2Ni_7D_{4.7-x}$ deuterides are presented in Table 4; selected interatomic distances are given in Table 5.

A complete rebuilding of the metal sublattice takes place within the $CeNi_2$ slabs. Fig. 4 illustrates the deformation of the metal sublattice that occurs inside these slabs during D uptake. Together with a huge expansion along the [001] direction, substantial shifts of both the central Ni1 atom and surrounding Ce atoms are observed. These shifts give rise to an orthorhombic distortion of the parent hexagonal structure. For Ni1, which is coordinated by the Ce_6 octahedron, the large unilateral expansion dramatically changes its coordination from 12 (Ce_6Ni_6) to 9 (Ce_6Ni_3).

The observed deformation of the metal sublattice is in agreement with the ordered deuterium locations in the structure as shown in Fig. 5. Deuterium atoms occupy six completely filled crystallographic sites, which are located inside the $CeNi_2$ slab, and three partially occupied sites lying on the boundary between $CeNi_2$ and $CeNi_5$ slabs. D atoms are almost evenly distributed among these three types of interstices: 1.5 at. D/f.u. in octahedra Ce_3Ni_3 (D1–D3), 1.5 at. D/f.u. in tetrahedra Ce_3Ni (D5, D6) and 1.65 at. D/f.u. in tetrahedra Ce_2Ni_2 (D4; D7–D9) (Fig. 6). Only the Ce_2Ni_2 interstitial sites exist in the structure of the original intermetallic compound; the Ce_3Ni and Ce_3Ni_3 interstices are formed via deformation of the metal sublattice induced by D atoms.

The D sublattice within the $CeNi_2$ slab is completely ordered; all D–D distances between completely filled D1–D6 sites D exceed 2.0 Å (1.9 Å in $Ce_2Ni_7D_{4.43}$). Local coordination of Ni by D atoms inside the $CeNi_2$ blocks is of an ''open'', saddle-like type within the layer formed from Ce_6 octahedra (Fig. 5 and Table 6). This shows a principal difference between $Ce_2Ni_7D_{4.7}$ and mixed

Table 3
Atomic parameters in the structure of the Ce_2Ni_7 intermetallic compound (space group: $P6_3/mmc$, $a = 4.94131(3)$ Å; $c = 24.5136(2)$ Å)

Atom	Site	x	y	z	U_{iso} (10^{-2} Å^2)
Ce1	4*f*	1/3	2/3	0.47021(4)	1.51(2)
Ce2	4*f*	1/3	2/3	0.32561(5)	0.97(2)
Ni1	2*a*	0	0	0	1.4(1)
Ni2	4*e*	0	0	0.3305(1)	0.33(5)
Ni3	4*f*	1/3	2/3	0.8182(7)	0.24(4)
Ni4	6*h*	0.8318(3)	2*x*	1/4	0.33(4)
Ni5	12*k*	0.8334(2)	2*x*	0.41529(5)	0.62(3)

Table 2
Crystallographic characteristics of the Ce_2Ni_7 compound and its deuterides

Compound	Ce_2Ni_7[a]	$Ce_2Ni_7D_{4.65(9)}$	$Ce_2Ni_7D_{4.43(9)}$
Space group	$P6_3/mmc$	$Pmcn$	$Pmcn$
Unit cell parameters (Å)	$a = 4.94131(3)$	$a = 4.9251(3)$	$a = 4.9146(3)$
	$c = 24.5136(2)$	$b = 8.4933(4)$	$b = 8.4651(5)$
		$c = 29.773(1)$	c = 29.629(1)
Unit cell volume (Å^3)	518.349(6)	1245.4(1)	1232.6(1)
Volume per formula unit (Å^3)	129.587(2)	155.68(1)	154.08(1)
H-induced deformation (%)			
$(b_{orth}/\sqrt{3}-a_{orth})/a_{orth}$	–	−0.44	−0.55
$\Delta c/c$	–	21.5	20.9
$\Delta V/V$	–	20.1	18.9
$\Delta c_{CeNi_2}/c_{CeNi_2}$	–	63.4	61.7
$\Delta V_{CeNi_2}/V_{CeNi_2}$	–	61.7	59.1
$\Delta c_{CeNi_5}/c_{CeNi_5}$	–	−0.02	−0.03
$\Delta V_{CeNi_5}/V_{CeNi_5}$	–	−1.11	−1.65
Source data	SXRD (293 K)	PND (2 MPa D_2, 293 K)	PND (0.1 MPa Ar, 293 K)
R-factors (%)			
R_{wp}	8.71	3.97	3.85
R_p	6.49	3.20	3.22
χ^2	9.46	2.90	4.44

[a]IMC after complete deuterium desorption from the deuteride.

Table 4
Atomic parameters in the structure of Ce_2Ni_7-based deuterides from Rietveld refinements of the powder neutron diffraction data

Atom[a]	Site	$Ce_2Ni_7D_{4.65(9)}$				$Ce_2Ni_7D_{4.43(9)}$			
		x	y	z	U_{iso}[b] (10^{-2} Å^2)	x	y	z	U_{iso}[b] (10^{-2} Å^2)
Ce1	4*c*	1/4	0.362(3)	0.0415(8)	2.8(3)	1/4	0.379(3)	0.0379(7)	2.8(3)
Ce2	4*c*	1/4	0.054(3)	0.9446(6)	2.8(3)	1/4	0.073(4)	0.9440(6)	2.8(3)
Ce3	4*c*	1/4	0.401(4)	0.1820(8)	0.9(2)	1/4	0.406(4)	0.1804(8)	1.5(2)
Ce4	4*c*	1/4	0.090(3)	0.8182(7)	0.9(2)	1/4	0.089(2)	0.8156(8)	1.5(2)
Ni1	4*c*	1/4	0.745(2)	0.0223(3)	1.0(2)	1/4	0.744(1)	0.0224(2)	0.5(1)
Ni2	4*c*	1/4	0.749(2)	0.1833(4)	1.2(1)	1/4	0.748(2)	0.1829(4)	1.1(1)
Ni3	4*c*	1/4	0.763(2)	0.8160(4)	1.2(1)	1/4	0.763(2)	0.8170(4)	1.1(1)
Ni4	4*c*	1/4	0.416(2)	0.8158(3)	0.7(1)	1/4	0.429(2)	0.8209(4)	0.3(1)
Ni5	4*c*	1/4	0.076(2)	0.1816(3)	0.7(1)	1/4	0.076(2)	0.1816(3)	0.3(1)
Ni6	4*c*	1/4	0.909(2)	0.2459(5)	1.2(1)	1/4	0.909(2)	0.2487(5)	1.20(8)
Ni7	8*d*	0.000(3)	0.833(2)	0.7463(3)	1.2(1)	0.006(3)	0.837(1)	0.7476(3)	1.20(8)
Ni8	4*c*	1/4	0.918(2)	0.3839(6)	1.18(6)	1/4	0.904(1)	0.3925(4)	0.90(5)
Ni9	4*c*	1/4	0.917(2)	0.1107(6)	1.18(6)	1/4	0.901(1)	0.1114(4)	0.90(5)
Ni10	8*d*	0.009(1)	0.840(1)	0.8856(4)	1.18(6)	−0.002(2)	0.847(1)	0.8838(3)	0.90(5)
Ni11	8*d*	0.501(2)	0.160(1)	0.3863(4)	1.18(6)	0.501(2)	0.164(1)	0.3861(3)	0.90(5)
D1	4*c*	1/4	0.103(3)	0.0808(7)	1.8(1)	1/4	0.088(3)	0.0768(6)	2.4(1)
D2	4*c*	1/4	0.779(3)	0.4215(5)	1.8(1)	1/4	0.746(3)	0.4184(5)	2.4(1)
D3	4*c*	1/4	0.080(4)	0.4196(6)	1.8(1)	1/4	0.079(4)	0.4176(5)	2.4(1)
D4	4*c*	1/4	0.606(2)	0.5507(6)	1.8(1)	1/4	0.628(2)	0.5588(6)	2.4(1)
D5	4*c*	1/4	0.580(3)	0.9990(6)	1.8(1)	1/4	0.584(3)	0.9969(5)	2.4(1)
D6	8*d*	0.529(3)	0.154(2)	0.0148(4)	1.8(1)	0.553(2)	0.146(2)	0.0152(4)	2.4(1)
D7[c]	8*d*	0.414(7) $n = 0.47(3)$	0.332(3)	0.111(1)	1.8(1)	0.433(8) $n = 0.34(3)$	0.357(7)	0.105(1)	2.4(1)
D8[c]	8*d*	0.422(8) $n = 0.33(3)$	0.493(5)	0.109(1)	1.8(1)	0.425(8) $n = 0.40(3)$	0.486(5)	0.108(1)	2.4(1)
D9[c]	8*d*	0.453(9) $n = 0.35(3)$	0.348(6)	0.391(1)	1.8(1)	–	–	–	–
D10[c]	4*c*	–	–	–	–	1/4 $n = 0.37(5)$	0.276(7)	0.382(2)	2.4(1)

$Ce_2Ni_7D_{4.65(9)}$. Space group: *Pmcn*; $a = 4.9251(3)$ Å; $b = 8.4933(4)$ Å; $c = 29.773(1)$ Å. $Ce_2Ni_7D_{4.43(9)}$. Space group: *Pmcn*; $a = 4.9146(3)$ Å; $b = 8.4651(5)$ Å; $c = 29.629(1)$ Å.

[a]Transformation from hexagonal to orthorhombic unit cell: (Ce1)→Ce1 and Ce2; (Ce2)→Ce3 and Ce4; (Ni1)→Ni1; (Ni2)→Ni2 and Ni3; (Ni3)→Ni4 and Ni5; (Ni4)→Ni6 and Ni7; (Ni5)→Ni8, Ni9, Ni10 and Ni11.

[b]U_{iso} parameters have been constrained to be equal for the chemically and structurally identical groups of atoms: Ce1 and Ce2; Ce3 and Ce4; Ni2 and Ni3; Ni4 and Ni5; Ni6 and Ni7; Ni8–Ni11; D1–D10.

[c]Partially occupied sites, *n*—site occupancy factor; when value of *n* is not stated, it equals to 1.

ionic-covalent-type hydrides having a partial negative charge on H, e.g. Mg_2NiH_4 [14], which contains tetrahedral $[NiH_4]^{4-}$ units.

Partially occupied D7, D8, D9 and D10 sites are located in the tetrahedral Ce_2Ni_2 sites between $MgZn_2$- and $CaCu_5$-type fragments. In total, the orthorhombic structure contains eight types of Ce_2Ni_2 tetrahedra connected into two types of Ce_2Ni_6 bipyramids. The occupancy/vacancy of these tetrahedral holes are dependent on the hole size. One type of Ce_2Ni_6 is built of Ce_2Ni_2 tetrahedra with radii of interstitial holes of 0.45–0.55 Å, whereas the other contains interstices with much smaller radii, 0.33–0.41 Å. Correspondingly, more deuterium atoms are located in the larger bipyramid, 0.80 D/f.u. (in D7 and D8 sites) compared to 0.35 D/f.u. (in D9) in the smaller one. In total, 6 of 8 types of Ce_2Ni_2 tetrahedra fulfil the size criterion (0.4 Å) to accommodate D atoms; however, due to short distances (blocking effect) between neighbouring sites, only 3 Ce_2Ni_2 sites are occupied in an ordered way. The size effect also explains the difference in Ce_2Ni_2 site occupation between $Ce_2Ni_7D_{4.65(9)}$ and $Ce_2Ni_7D_{4.43(9)}$ (see Table 4 for details). In the $Ce_2Ni_7D_{4.43(9)}$ structure the D9 site (8*f*) becomes too small (unit cell is smaller) to accommodate D atoms (less than 0.4 Å), and a sufficiently large neighbouring D10 site (0.40 Å) is occupied instead (0.18 D/f.u.). Thus, 1.65 D/f.u. are located in the Ce_2Ni_2 sites in the saturated $Ce_2Ni_7D_{4.65(9)}$ deuteride and 1.43 D/f.u. in $Ce_2Ni_7D_{4.43(9)}$.

The hydrogenation behaviour of the constituent parts of $CeNi_5$ and $CeNi_2$, reveals differences in comparison with the corresponding binary intermetallic compounds. The $CeNi_2$ cubic Laves-phase becomes amorphous on hydrogenation [15] while the $CeNi_5$-based hydride at room temperature decomposes at pressures below 48 bar [16]. In contrast, the $CeNi_5$ units stabilise the $CeNi_2$ layers in Ce_2Ni_7 and a well crystalline $Ce_2Ni_7D_{4.7}$ is formed. Instead of filling the existing interstitial sites, deuterium (hydrogen) induces structural transformations leading to the creation

Table 5
Selected interatomic distances (Å) in the crystal structures of the Ce_2Ni_7-based deuterides

Atoms	$Ce_2Ni_7D_{4.65(9)}$	$Ce_2Ni_7D_{4.43(9)}$
D1…Ce1	2.49(4)	2.72(3)
D1…Ce2 × 2	2.90(2)	2.88(2)
D1…Ni9	1.81(3)	1.89(3)
D1…Ni10 × 2	1.69(2)	1.77(2)
D2…Ce1 × 2	2.78(2)	2.99(2)
D2…Ce2	2.91(3)	2.80(4)
D2…Ni8	1.63(2)	1.55(2)
D2…Ni10 × 2	1.89(2)	1.79(1)
D3…Ce1 × 2	3.29(3)	3.26(2)
D3…Ce2	3.20(4)	3.05(5)
D3…Ni8	1.74(3)	1.65(3)
D3…Ni11 × 2	1.72(2)	1.71(2)
D4…Ce2 × 2	2.505(5)	2.501(7)
D4…Ni1	1.53(3)	1.53(1)
D4…Ni9	1.80(2)	1.58(2)
D5…Ce1	2.25(4)	2.18(2)
D5…Ce1 × 2	2.79(1)	2.68(1)
D5…Ni1	1.56(3)	1.55(2)
D6…Ce1	2.37(3)	2.56(3)
D6…Ce2	2.64(2)	2.66(2)
D6…Ce2	2.40(3)	2.41(3)
D6…Ni1	1.78(2)	1.75(1)
D7…Ce1	2.23(4)	2.20(3)
D7…Ce3	2.35(4)	2.44(4)
D7…Ni8	1.82(4)	1.61(4)
D7…Ni10	1.53(3)	1.79(5)
D8…Ce1	2.45(5)	2.42(5)
D8…Ce3	2.45(4)	2.41(4)
D8…Ni8	1.75(5)	1.74(3)
D8…Ni11	1.47(4)	1.56(4)
D9…Ce2	2.07(5)	–
D9…Ce4	2.43(5)	–
D9…Ni9	1.58(5)	–
D9…Ni11	1.62(5)	–
D10…Ce2	–	2.24(6)
D10…Ce4	–	2.28(6)
D10…Ni11 × 2	–	1.56(3)

of significantly different environments for hydrogen atoms in $Ce_2Ni_7D_{4.7}$ in comparison with the initial intermetallic alloys $CeNi_5$ and $CeNi_2$.

With deuteration, very similar changes were previously observed in the $CeNi_2$ slab of the orthorhombic $CeNi_3D_{2.8}$ structure [2]. However, $CeNi_3D_{2.8}$ is characterised by a much larger degree of orthorhombic distortion, $(b_{orth}/\sqrt{3}-a_{orth})/a_{orth} = 1.37\%$, compared to $Ce_2Ni_7D_{4.65}$ (−0.44%). This can be explained by different ratios of $CaCu_5$- and $MgZn_2$-type slabs in the $CeNi_3$ and Ce_2Ni_7 units (1:2 and 1:1, respectively). Twice as large and containing no hydrogen, $CeNi_5$ units make the metal matrix of Ce_2Ni_7 more rigid to orthorhombic deformation.

The D sublattice of the $Ce_2Ni_7D_{4.7}$ structure is similar to that of $CeNi_3D_{2.8}$. In both cases, there are six fully occupied D sites in the $CeNi_2$ slabs giving 3.5 at. D/$CeNi_2$. Five of these six sites are equivalent in both deuterides. One significant difference for $Ce_2Ni_7D_{4.7}$ is in occupancy of the D4 site (Ce_2Ni_2), which is adjacent to the octahedron Ce_2Ni_4 (D6 site) occupied by D in $CeNi_3D_{2.8}$ [2]. This difference changes the local coordination of Ni by D atoms inside the $CeNi_2$ blocks: a tetrahedral NiD_4 coordination which can be concluded for Ni1 in the crystal structure of $CeNi_3D_{2.8}$ [2] (Ni1D3D5$_2$D6; Ni–D = 1.55–1.56 Å) is changed to the saddle-like-type NiD_4 units in $Ce_2Ni_7D_{4.7}$. Interestingly, saddle-type coordination is not known for the Ni-based complex hydrides [17]; however, it has been reported for various transition metals including Co in $Mg_6Co_2D_{11}$ [18] and Ru in Mg_2RuH_4 [19]. However, a wide variation in the Ni–D distances in $Ce_2Ni_7D_{4.7}$, from 1.53 to 1.78 Å, contrasts to a rather narrow range of transition metal-to-hydrogen distances observed for the tetrahedral $[NiH_4]^{4-}$ in Mg_2NiH_4 (1.519–1.572 Å) [13], and for saddle-like CoH_4 in $Mg_6Co_2H_{11}$ (1.521–1.603 Å) [18], and RuH_4 in Mg_2RuH_4 (1.665–1.681 Å) [19]. This difference is an argument in favour of absence of the formation of NiH_n complexes in the studied $Ce_2Ni_7D_{4.7}$ deuteride.

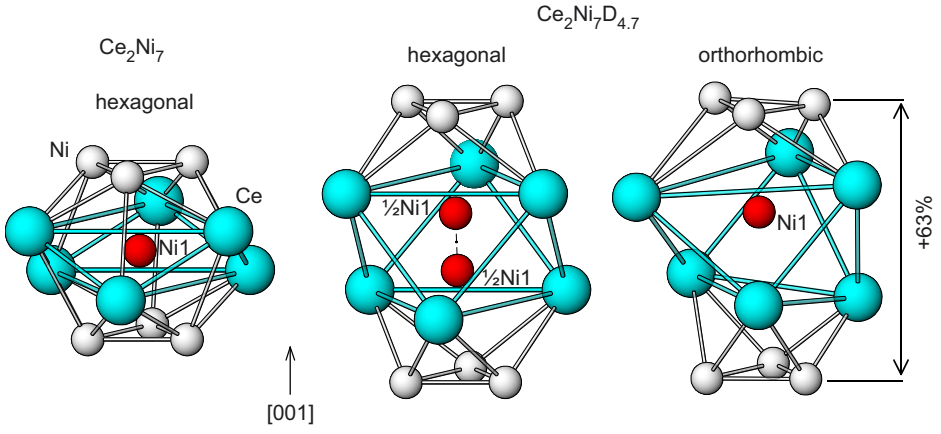

Fig. 4. Changes in coordination polyhedron of Ni1 during hydrogen absorption. The large unilateral expansion along the *c*-axis dramatically changes coordination from 12 (Ce_6Ni_6) to 9 (Ce_6Ni_3), and there is an extremely pronounced deformation of the layer formed by Ce_6 octahedra centred on Ni1. A hexagonal description of the structure allows for a split site with all Ni1 sites 50% occupied; the distance between those split sites is 1.4 Å. Note that for an orthorhombic unit cell the Ni1 atom shifts from the centre of the Ce_6 octahedra and fills one of the equivalent split sites in an ordered way; the other site is vacant.

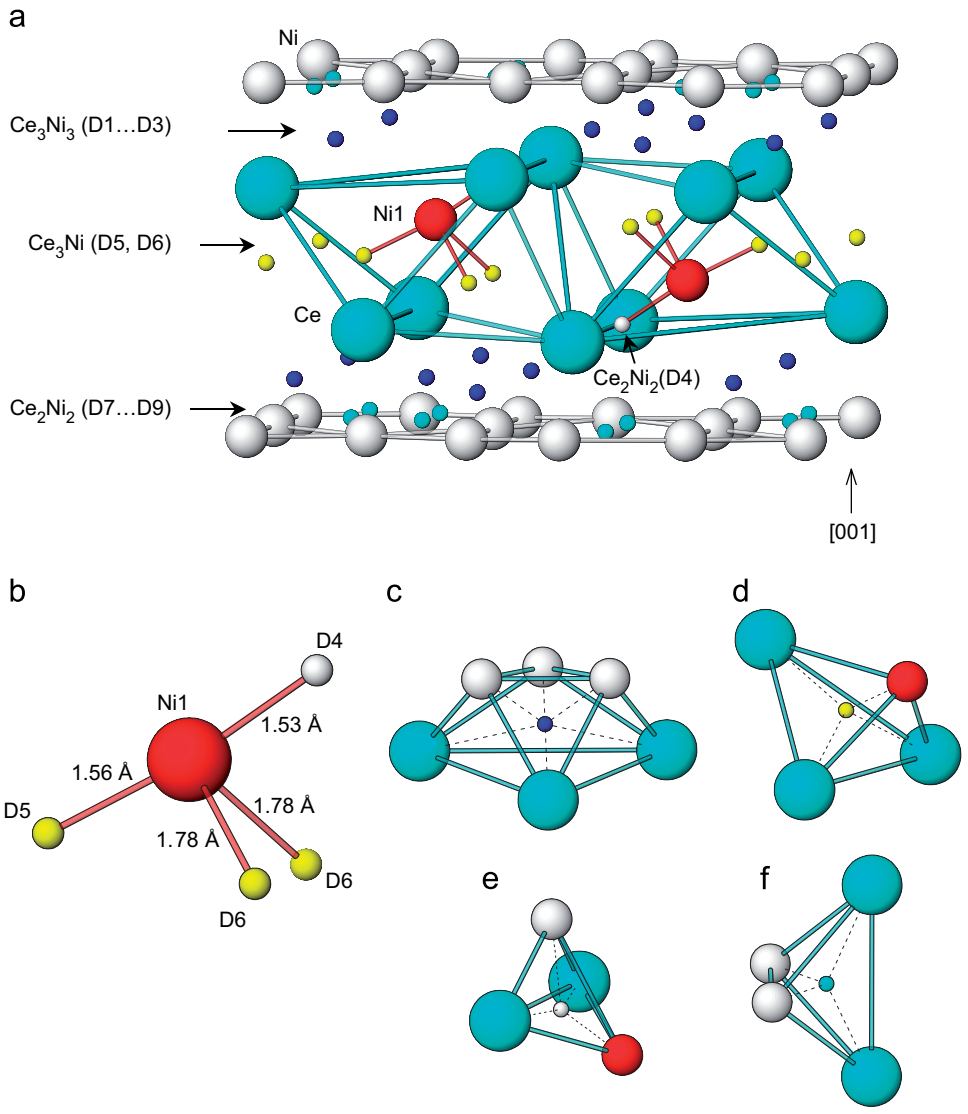

Fig. 5. $CeNi_2$ ($MgZn_2$-type) slab in the crystal structure of $Ce_2Ni_7D_{4.7}$: (a) showing the ordered D sublattice; (b) saddle-like coordination of Ni1 by 4 D atoms (within the layer formed from Ce_6 octahedra). Four types of D-occupied sites are shown: (c) deformed octahedra Ce_3Ni_3; (d) tetrahedra Ce_3Ni; (e) tetrahedra Ce_2Ni_2. These sites are occupied by D1–D6 and are completely filled. D7–D9 atoms partially fill the Ce_2Ni_2 sites (f) located on the interface between $CeNi_2$ ($MgZn_2$-type) and $CeNi_5$ ($CaCu_5$-type) slabs.

The existence of the specific MH_x coordination in structures of metal hydrides is necessary but far not sufficient criterion for considering a hydride as the complex one. Because of variety of Ni coordinations by H atoms, these anisotropic hydrides cannot be considered as genuine complex hydrides, which are formed in the systems of alkaline (alkaline earth or magnesium) and transition metals with hydrogen.

In the Kagome nets formed by Ni atoms, which are located on the border between $CeNi_2$ and $CeNi_5$, D content is very similar, 1.3 at. D/f.u. ($CeNi_3$) or 1.15 at. D/f.u. (Ce_2Ni_7). Different types of the Ce_2Ni_2 tetrahedral interstitial positions are occupied leading to differences in ordering of the hydrogen sublattice. Maximum possible H(D) content in these nets equals to 3.0 at. H/Ce_2Ni_7 leading to a possibility of reaching 6.5 at. H/f.u. Ce_2Ni_7 as a limiting value (3.5 at. H inside the $CeNi_2$ slab + 3.0 at. H on the border of $CeNi_2$ and $CeNi_5$; hydrogen sublattice will be different for the former layers from that experimentally observed in $Ce_2Ni_7D_{4.7}$).

Comparison of the results obtained in present work during studies of the Ce_2Ni_7-based hydrides and in the previous publication by Filinchuk et al. [6] shows similar features in the structure of the metal matrix of the hydrides. However, a smaller deuterium content (4.1D/Ce_2Ni_7) and a rather different deuterium substructure was reported [6]. These differences can be caused by the methods of preparation and handling of the sample in [6]. Indeed, exposure of the samples to air may lead to the chemical reaction of the hydride with O_2/N_2/water vapour causing hydrogen release, which would modify structural properties of the material. Such a reaction may result in the observed inhomogeneity of the material [6]; several coexisting Ce_2Ni_7-based hydride phases were identified.

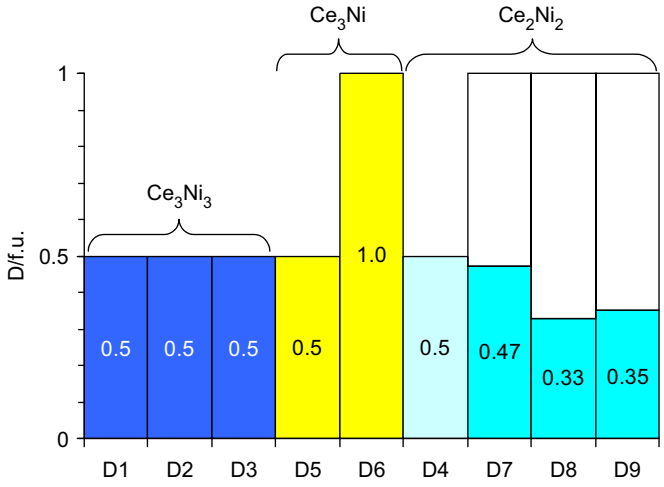

Fig. 6. Distribution of deuterium atoms in the structure of $Ce_2Ni_7D_{4.7}$ deuteride. Three different groups of sites are shown: octahedral D1–D3 and tetrahedral D4–D6 sites located inside the $CeNi_2$ slab, D7–D9 sites located in Ce_2Ni_2 tetrahedra on the interface between $CeNi_2$ and $CeNi_5$. The occupation of each D site is given in the fraction of atoms D/f.u.; the sum of these occupations is equal to the overall stoichiometry for each deuteride.

Table 6
Interatomic distances Ni1⋯D (Å) and angles D⋯Ni1⋯D (°)

Atoms	$Ce_2Ni_7D_{4.65(9)}$	$Ce_2Ni_7D_{4.43(9)}$
Ni1…D4	1.53(3)	1.53(1)
Ni1…D5	1.56(3)	1.55(2)
Ni1…D6 × 2	1.78(2)	1.75(1)
D4…Ni1…D5	173(1)	164(1)
D4…Ni1…D6 × 2	87(1)	94.1(9)
D5…Ni1…D6 × 2	99.1(8)	99.0(7)
D6…Ni1…D6	76(1)	67.3(7)

These phases also included a small quantity of the intermetallic alloy in the sample, which can be formed during completion of the H desorption from the hydride and which was indeed observed in the diffraction pattern. Possibly for these reasons, refinements of the structure of $Ce_2Ni_7D_{4.1}$ [6] yielded an unreliably short Ni–D distance of 1.38 Å and incomplete coordination of one of the D sites by the metal atoms (D7: with only two Ce atoms as closest neighbours, which form a nonlinear Ce–D–Ce unit) [6]. These features raise questions concerning the proposed hydrogen (deuterium) sublattice. Certainly, only *in situ* experiments under different selected pressures of $D_2(H_2)$ can confirm the proposed formation of the tetrahedral NiD_4 coordination [6].

Anomalous structural behaviour of anisotropic $RENi_3$- and RE_2Ni_7-based hydrides requires further studies to understand the mechanism of their formation. Such behaviour in all studied hydrides correlates with D ordering in the metallic matrix and preferential filling of interstitial sites coordinated mostly by RE atoms (RE_3Ni, RE_3Ni_3 and RE_2Ni_2). Obviously, the RE–H interactions play the most important role in hydrogen-induced structural transformation in the RE–Ni compounds. Theoretical first principal calculations will be of high value to probe the nature of the metal–hydrogen bonding in anisotropic hydrides and to address the question of hydrogen ordering and stabilisation of specific clusters containing RE, Ni and H atoms.

In conclusion, this study shows that anisotropic $Ce_2Ni_7D_{4.7}$ deuteride resembles structural features characteristic for the hydrogenation of the $RENi_3$ (RE = La, Ce) and RE_2Ni_7 (RE = La) intermetallic alloys. These include:

1. Expansion during H absorption proceeds exclusively within the $RENi_2$ layers and is caused by hydrogen atoms occupying these slabs.
2. The D atoms fill the sites where contribution from the active hydride-forming element La or Ce into their surrounding is high (octahedra RE_3Ni_3, tetrahedra RE_3Ni and tetrahedra RE_2Ni_2), not less than 50%.
3. Hydrogen sublattice within the $RENi_2$ slabs is completely ordered. However, types of the D ordering vary depending on the compound; $Ce_2Ni_7D_{4.7}$: saddle-type coordination NiD_4; $CeNi_3D_{2.8}$: tetrahedron NiD_4; $La_2Ni_7D_{6.5}$ and $LaNi_3D_{2.8}$: octahedra NiD_6. Thus, coordination of Ni by D has a variety of forms with Ni–D distances changing in a broad range indicating that formation of Ni–H complexes is rather unlikely.
4. Unusual thermodynamic behaviour of the Ce_2Ni_7-based hydride reflects its association with a group of anisotropic hydrides where metal–hydrogen bonding is expected to be significantly different from the traditional insertion-type intermetallic hydrides.

Acknowledgements

This work was supported by the Nordic Energy Research (Project 46-02 NORSTORE) and NEDO, Japan (Project "Novel Intermetallic Hydrides with High Volume Density and Advanced Surface Properties" between IFE and Tokai University). We wish to thank H. Emerich and W. van Beek for their skilful assistance during the SR-XRD experiments at the Swiss–Norwegian Beam Lines.

References

[1] V.A. Yartys, A.B. Riabov, R.V. Denys, M. Sato, R.G. Delaplane, J. Alloys Compds. 408–412 (2006) 273–279.
[2] V.A. Yartys, O. Isnard, A.B. Riabov, L.G. Akselrud, J. Alloys Compds. 356/357 (2003) 109–113.
[3] R.V. Denys, A.B. Riabov, V.A. Yartys, R.G. Delaplane, M. Sato, J. Alloys Compd. (2006), in press, doi:10.1016/j.jallcom.
[4] M. Latroche, V. Paul-Boncour, A. Percheron-Guegan, J. Solid State Chem. 177 (7) (2004) 2542–2549.
[5] K.H.J. Buschow, A.S. van der Goot, J. Less-Common Met. 22 (1970) 419–428.
[6] Y.E. Filinchuk, K. Yvon, H. Emerich, Inorg. Chem. 46 (7) (2007) 2914–2920.

[7] D.T. Cromer, A.C. Larson, Acta Crystallogr. 12 (1959) 855–859.
[8] A. Wannberg, M. Gronros, A. Mellergard, L.-E. Karlson, R.G. Delaplane, B. Lebech, Z. Kristallogr. Suppl. 23 (2006) 195–198.
[9] A.C. Larson, R.B. von Dreele, General Structure Analysis System (GSAS), LANSCE, MS-H, vol. 805, 1994.
[10] R.H. van Essen, K.H.J. Buschow, J. Less-Common Met. 70 (1980) 189–198.
[11] M. Sato, V.A. Yartys, J. Alloys Compds. 373 (2004) 161–166.
[12] C.E. Lundin, F.E. Lynch, C.B. Magee, J. Less Common Met. 56 (1977) 19–37.
[13] M.D. Chio, S. Livraghi, M. Baricco, J. Alloys Compds. 426 (2006) 180–185.
[14] P. Zolliker, K. Yvon, J.D. Jorgensen, F.J. Rotella, Inorg. Chem. 25 (20) (1986) 3590–3593.
[15] V. Paul-Boncour, C. Lartigue, A. Percheron-Guegan, J.C. Achard, J. Pannetier, J. Less-Common Met. 143 (1988) 301–313.
[16] F. Pourarian, W.E. Wallace, Int. J. Hydr. Energy 10 (1) (1985) 49–58.
[17] R. Bau, M.H. Drabnis, Inorg. Chim. Acta 259 (1997) 27–50.
[18] R. Cerny, F. Bornhomme, K. Yvon, P. Fischer, P. Zolliker, D.E. Cox, A. Hewat, J. Alloys Compds. 187 (1992) 233–241.
[19] F. Bornhomme, K. Yvon, G. Triscone, K. Jansen, G. Auffermann, P. Muller, W. Bronger, J. Alloys Compds. 178 (1992) 161–166.